Exchange-coupling-induced fourfold magnetic anisotropy in CoFeB/FeRh bilayer grown on $SrTiO_3$(001)

Qingrong Shao(邵倾蓉), Jing Meng(孟婧), Xiaoyan Zhu(朱晓艳), Yali Xie(谢亚丽), Wenjuan Cheng(程文娟), Dongmei Jiang(蒋冬梅), Yang Xu(徐杨), Tian Shang(商恬), and Qingfeng Zhan(詹清峰)

Citation: Chin. Phys. B, 2022, 31 (**8**): 087503. DOI: 10.1088/1674-1056/ac673c
Journal homepage: http://cpb.iphy.ac.cn; http://iopscience.iop.org/cpb

What follows is a list of articles you may be interested in

Voltage control magnetism and ferromagnetic resonance in an $Fe_{19}Ni_{81}$/PMN-PT heterostructure by strain

Jun Ren(任军), Junming Li(李军明), Sheng Zhang(张胜), Jun Li(李骏), Wenxia Su(苏文霞), Dunhui Wang(王敦辉), Qingqi Cao(曹庆琪), and Youwei Du(都有为)

Chin. Phys. B, 2022, 31 (**7**): 077502. DOI: 10.1088/1674-1056/ac43ab

Non-volatile multi-state magnetic domain transformation in a Hall balance

Yang Gao(高阳), Jingyan Zhang(张静言), Pengwei Dou(窦鹏伟), Zhuolin Li(李卓霖), Zhaozhao Zhu(朱照照), Yaqin Guo(郭雅琴), Chaoqun Hu(胡超群), Weidu Qin(覃维都), Congli He(何聪丽), Shipeng Shen(申世鹏), Ying Zhang(张颖), and Shouguo Wang(王守国)

Chin. Phys. B, 2022, 31 (**6**): 067502. DOI: 10.1088/1674-1056/ac65f5

Perpendicular magnetization and exchange bias in epitaxial NiO/$[Ni/Pt]_2$ multilayers

Lin-Ao Huang(黄林傲), Mei-Yu Wang(王梅雨), Peng Wang(王鹏), Yuan Yuan(袁源), Ruo-Bai Liu(刘若柏), Tian-Yu Liu(刘天宇), Yu Lu(卢羽), Jia-Rui Chen(陈家瑞), Lu-Jun Wei(魏陆军), Wei Zhang(张维), Biao You(游彪), Qing-Yu Xu(徐庆宇), and Jun Du(杜军)

Chin. Phys. B, 2022, 31 (**2**): 027506. DOI: 10.1088/1674-1056/ac2b22

Probing the magnetization switching with in-plane magnetic anisotropy through field-modified magnetoresistance measurement

Runrun Hao(郝润润), Kun Zhang(张昆), Yinggang Li(李迎港), Qiang Cao(曹强), Xueying Zhang(张学莹), Dapeng Zhu(朱大鹏), and Weisheng Zhao(赵巍胜)

Chin. Phys. B, 2022, 31 (**1**): 017502. DOI: 10.1088/1674-1056/ac21bb

Perpendicular magnetic anisotropy of Pd/Co_2MnSi/$NiFe_2O_4$/Pd multilayers on F-mica substrates

Qingwang Bai(白青旺), Bin Guo(郭斌), Qin Yin(尹钦), and Shuyun Wang(王书运)

Chin. Phys. B, 2022, 31 (**1**): 017501. DOI: 10.1088/1674-1056/ac20cc

---

Exchange-coupling-induced fourfold magnetic anisotropy in CoFeB/FeRh bilayer grown on $SrTiO_3$(001)

Qingrong Shao(邵倾蓉)[1], Jing Meng(孟婧)[1], Xiaoyan Zhu(朱晓艳)[1], Yali Xie(谢亚丽)[2], Wenjuan Cheng(程文娟)[1], Dongmei Jiang(蒋冬梅)[1], Yang Xu(徐杨)[1], Tian Shang(商恬)[1], and Qingfeng Zhan(詹清峰)[1,†]

[1] *Key Laboratory of Polar Materials and Devices (MOE), School of Physics and Electronic Science, East China Normal University, Shanghai* 200241, *China*

[2] *Key Laboratory of Magnetic Materials and Devices, Ningbo Institute of Material Technology and Engineering, Chinese Academy of Sciences, Ningbo* 315201, *China*

(Received 22 February 2022; revised manuscript received 5 April 2022; accepted manuscript online 14 April 2022)

Exchange coupling across the interface between a ferromagnetic (FM) layer and an antiferromagnetic (AFM) or another FM layer may induce a unidirectional magnetic anisotropy and/or a uniaxial magnetic anisotropy, which has been extensively studied due to the important application in magnetic materials and devices. In this work, we observed a fourfold magnetic anisotropy in amorphous CoFeB layer when exchange coupling to an adjacent FeRh layer which is epitaxially grown on an $SrTiO_3$(001) substrate. As the temperature rises from 300 K to 400 K, FeRh film undergoes a phase transition from AFM to FM phase, the induced fourfold magnetic anisotropy in the CoFeB layer switches the orientation from the FeRh⟨110⟩ to FeRh⟨100⟩ directions and the strength is obviously reduced. In addition, the effective magnetic damping as well as the two-magnon scattering of the CoFeB/FeRh bilayer also remarkably increase with the occurrence of magnetic phase transition of FeRh. No exchange bias is observed in the bilayer even when FeRh is in the nominal AFM state, which is probably because the residual FM FeRh moments located at the interface can well separate the exchange coupling between the below pinned FeRh moments and the CoFeB moments.

Keywords: magnetic anisotropy, phase transition, CoFeB/FeRh, exchange coupling

PACS: 75.30.Gw, 75.50.Ee, 75.50.Gg, 75.60.Nt **DOI:** 10.1088/1674-1056/ac673c

1. Introduction

Magnetic anisotropy is a very important parameter in the application of magnetic thin film devices, which has intrinsic and extrinsic origins. When magnetic materials with cubic structure is epitaxially grown on single crystal substrates, an in-plane fourfold magnetic anisotropy can be observed due to its intrinsic cubic magnetocrystalline anisotropy, such as Fe/MgO(001)[1] and Fe_3O_4/GaAs(100).[2] In contrast, an amorphous magnetic film cannot show the intrinsic magnetocrystalline anisotropy due to the absence of long-range order in the crystal lattice. Extrinsic magnetic anisotropies can be resulted from various origins, such as shape of materials,[3] mechanical stress,[4,5] and interfacial exchange coupling.[6,7] The last case is prevalent in designing and fabricating magnetic materials and devices. When a ferromagnetic (FM) layer is exchange coupled to an antiferromagnetic (AFM) layer, a hysteresis loop shift and a coercivity enhancement are often observed. This kind of exchange bias (EB) coupling can induce a unidirectional anisotropy and an extra uniaxial anisotropy, for which reason the AFM materials are widely used in spintronic devices as a pinning layer.[8–12] When a soft FM layer with high saturation magnetization is exchange coupled to a hard FM layer with high coercivity, the composite materials may display a high magnetic energy product. This kind of exchange spring coupling is usually employed to design the next generation of permanent magnet materials.[13–15] Although the fourfold magnetic anisotropy is often obtained through the epitaxial growth of an FM layer with cubic structure, it cannot be induced by the interfacial exchange coupling regardless at the FM/AFM or FM/FM interfaces. Different from the exchange-coupling-induced magnetic anisotropy, the fourfold magnetic anisotropy of epitaxial magnetic films is not easy to be tuned due to its intrinsic nature.

The CsCl-type FeRh alloy is AFM at room temperature, undergoes a first-order phase transition to FM as the temperature rises around 370 K,[16–19] and shows a coexistence of AFM and FM phases during the transition. The peculiar magnetic transition gives FeRh film potential application in thermally assisted magnetic recording storage.[20] When an AFM FeRh layer is proximate to a hard FM media of FePt layer, the exchange bias coupling occurring at the interface can increase the coercivity of FePt, thus improve the stability of magnetic information storage. After the occurrence of magnetic transition of FeRh at an elevated temperature, the exchange spring coupling between the FM FeRh and the FePt layer can significantly reduce the coercivity of FePt, thus enable the information writing with a low magnetic field.

Soft FM material of CoFeB displays the excellent mag-

†Corresponding author. E-mail: qfzhan@phy.ecnu.edu.cn

netic properties such as high spin polarization, high permeability, low coercivity, and low magnetic damping[21–23] due to the unique amorphous structure with the absence of dislocations and grain boundaries.[24,25] Consequently, CoFeB in the form of thin film has been widely used in spintronic devices.[22,23,26–29] Due to the lack of crystal structure, amorphous CoFeB film has no magnetocrystalline anisotropy, but usually reveals a weak uniaxial anisotropy.[30] In this paper, we realized an unusual fourfold magnetic anisotropy in amorphous CoFeB layer by means of exchange coupling to an adjacent FeRh layer which is epitaxially grown on $SrTiO_3$(001) substrate. As the temperature increases, FeRh transfers from AFM to FM states, the induced fourfold magnetic anisotropy of the CoFeB layer switches the orientation from FeRh⟨100⟩ to FeRh⟨100⟩ directions, and the strength is obviously reduced.

2. Experiment

CoFeB(15 nm)/FeRh(50 nm) bilayer was grown onto (001) oriented $SrTiO_3$ (STO) substrate by using an ultrahigh vacuum magnetron sputtering system with a base pressure lower than 1.0×10^{-8} Torr (1 Torr = 1.33322×10^{2} Pa). The STO substrate was pre-annealed at 700 °C for an hour and held at 750 °C during deposition. FeRh layer was sputtered from a stoichiometric $Fe_{50}Rh_{50}$ target in an argon atmosphere of 3 mTorr, and then was subjected to *in situ* annealing at 780 °C for 90 min to promote the atomic ordering. After naturally cooled to room temperature, $Co_{40}Fe_{40}B_{20}$ (CoFeB) layer was deposited on top of the FeRh layer. Reference FeRh(50 nm) and CoFeB(15 nm) single layers were grown on STO(001) by using the same growth parameters. All the samples were coated with a 3-nm Ta layer at room temperature to avoid oxidation before being taken out of the vacuum chamber. X-ray diffraction (XRD) θ–2θ and Φ-scans were performed to characterize the crystalline structure and the epitaxial nature. Magnetic property measurement system (MPMS, Quantum Design) was used to characterize the magnetic phase transition. Magneto-optical Kerr effect (MOKE) setup was used to characterize the hysteresis loops at various in-plane orientations of magnetic field. Ferromagnetic resonance (FMR) measurements were carried out to obtain the magnetic anisotropy and the magnetic damping parameters.

3. Result and discussion

Figure 1(a) shows the x-ray diffraction θ–2θ pattern of the CoFeB/FeRh bilayer grown on STO(001) substrate. The FeRh(001) and (002) diffraction peaks are clearly seen, indicating the formation of CsCl-type ordered structure with a (001)-preferential growth orientation. No CoFeB peak is detected due to the amorphous structure. The x-ray Φ-scan pattern displays four peaks separated by 90° for both STO substrate and FeRh layer, as shown in Fig. 1(b). The two sets of peaks have a 45° deviation, thus the epitaxial relationship is known to be STO(001)[010]||FeRh(001)[110], as shown in Fig. 1(c). Before the subsequent temperature-dependent magnetization (M–T) measurement, a 1-T field cooling process was performed along the STO[100] orientation. The saturation magnetization of the bilayer increases from 415 emu/cc at 300 K to 1075 emu/cc at 400 K, which confirms the presence of antiferromagnetic (AFM) to ferromagnetic (FM) phase transition of FeRh,[17,31] as shown in Fig. 1(d). The reference CoFeB single layer was measured to show a magnetization of 996 emu/cc at 300 K and a slightly reduced value of 964 emu/cc at 400 K. The magnetization of FeRh layer is 143 emu/cc at 300 K and 898 emu/cc at 400 K. The residual magnetization in the AFM state is often observed to be located within 6 nm–8 nm near the top and bottom interfaces of FeRh layer,[32–36] because the presence of antisite defects at the interfaces results in some neighboring Fe–Fe atom pairs changing to FM coupling.[32] The residual magnetization of FeRh grown on STO(001) is slightly larger than that on MgO(001).[32,35] According to the lattice parameters $\alpha_{FeRh} = 0.2995$ nm, $\alpha_{STO} = 0.3905$ nm, and $\alpha_{MgO} = 0.4216$ nm, FeRh film is subjected to a compressive strain of 0.53% when epitaxially grown on MgO(001) substrate, while the compressive strain remarkably increases to 7.8% for FeRh on STO(001).[37] This epitaxial strain can be relaxed through the formation of structural defects.

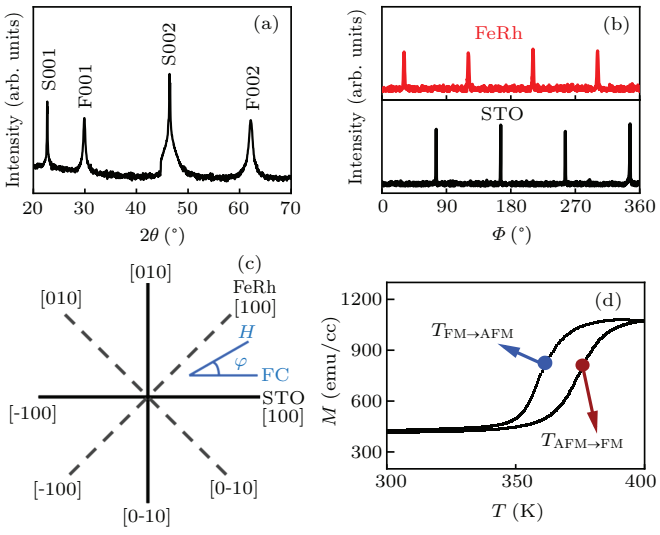

Fig. 1. X-ray (a) θ–2θ scan and (b) Φ scan of the CoFeB/FeRh bilayer grown on STO(001) substrate. The S and F marked on the diffraction peaks indicate STO and FeRh, respectively. (c) Schematic diagram of the epitaxial relationship between FeRh and STO lattices. A 1-T field cooling process was performed along STO[100], then an in-plane external field was applied in subsequent measurements at different angles φ with respect to STO[100]. (d) Temperature dependence of magnetization of the CoFeB/FeRh bilayer. The critical temperatures of phase transition in the heating and cooling branches are indicated as well.

Consequently, the large epitaxial strain imposed by STO substrate may lead to a large residual magnetization of FeRh in

the AFM state. By taking a derivative of the M–T curves, the AFM–FM transition temperatures in the heating and cooling branches are extracted as $T_{\mathrm{AFM}\to\mathrm{FM}} = 375$K and $T_{\mathrm{FM}\to\mathrm{AFM}} = 359$ K, respectively. The thermal hysteresis, *i.e.*, the difference between $T_{\mathrm{AFM}\to\mathrm{FM}}$ and $T_{\mathrm{FM}\to\mathrm{AFM}}$, clearly indicates the first-order of phase transition of FeRh.

Hysteresis loops were measured by MOKE at 300 K and 400 K with a magnetic field applied in film plane at various angles φ with respect to the STO[100] direction, *i.e.*, the FeRh$[1\bar{1}0]$ direction. The measurements at 300 K were conducted after a 1-T field cooling process in MPMS from 400 K. The MOKE signal comes from the upper CoFeB layer because the laser illuminates the sample from the top side, the 10-nm penetration depth of the used He–Ne laser is lower than the thickness of CoFeB.[38] As shown in Fig. 2(a), the hysteresis loop measured at $\varphi = 0°$ displays a large squareness $M_{\mathrm{r}}/M_{\mathrm{s}} = 0.92$ and a large coercivity $H_{\mathrm{c}} = 60$ Oe (1 Oe = 79.5775 A·m^{-1}), while the hysteresis loop measured at $\varphi = 45°$ is sheared with a low $M_{\mathrm{r}}/M_{\mathrm{s}} = 0.75$ and a small $H_{\mathrm{c}} = 30$ Oe.

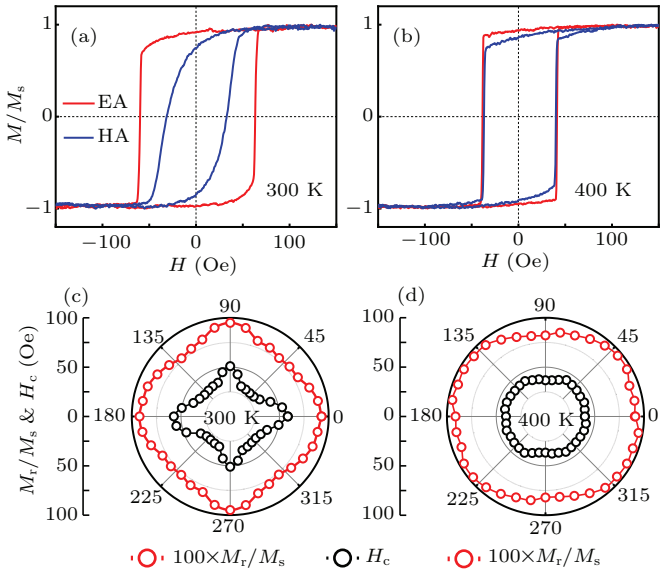

Fig. 2. Hysteresis loops of the CoFeB/FeRh bilayer obtained with an external magnetic field applied along the easy axis (EA) and the hard axis (HA) at (a) 300 K and (b) 400 K. Angular dependence of normalized $M_{\mathrm{r}}/M_{\mathrm{s}}$ and H_{c} of the bilayer measured at (c) 300 K and (d) 400 K.

Figures 2(b) shows the hysteresis loops measured at the same two magnetic field orientations at 400 K. The hysteresis loop at $\varphi = 0°$ changes to a relatively sheared one with $M_{\mathrm{r}}/M_{\mathrm{s}} = 0.85$ and $H_{\mathrm{c}} = 40$ Oe. Meanwhile, the hysteresis loop at $\varphi = 45°$ changes to a relatively square one with $M_{\mathrm{r}}/M_{\mathrm{s}} = 0.94$ and $H_{\mathrm{c}} = 42$ Oe. Figures 2(c) and 2(d) show the angular dependence of $M_{\mathrm{r}}/M_{\mathrm{s}}$ and H_{c} extracted from the hysteresis loops obtained at 300 K and 400 K, respectively. Both $M_{\mathrm{r}}/M_{\mathrm{s}}$ and H_{c} reveal an in-plane fourfold symmetry. At 300 K when FeRh is in the AFM state, the maximum values appear at $\varphi = 0°$, 90°, 180°, and 270°, *i.e.*, the in-plane FeRh⟨110⟩ directions. While the minimum values are located at $\varphi = 45°$, 135°, 225°, and 315°, *i.e.*, the in-plane FeRh⟨100⟩ directions. Because the angular dependence of $M_{\mathrm{r}}/M_{\mathrm{s}}$ and H_{c} are direct consequence of magnetic anisotropy, the symmetry of $M_{\mathrm{r}}/M_{\mathrm{s}}$ and H_{c} indicates that when exchange coupling to an AFM FeRh layer, the amorphous CoFeB layer displays a fourfold magnetic anisotropy with the easy axes orienting along the FeRh⟨110⟩ direction and the hard axes along the FeRh⟨100⟩ direction. At 400 K when FeRh enters into the FM state, the maximum values of both $M_{\mathrm{r}}/M_{\mathrm{s}}$ and H_{c} change to appear at $\varphi = 45°$, 135°, 225°, and 315°. The minimum values are located at $\varphi = 0°$, 90°, 180°, and 270°. Thus, the easy and hard axes of the fourfold magnetic anisotropy in CoFeB layer change to orient along the FeRh⟨100⟩ and ⟨110⟩ directions, respectively. In contrast, the reference CoFeB single film grown on STO(001) displays a clear uniaxial magnetic anisotropy and the reference FeRh single film in the FM state reveals a fourfold magnetic anisotropy.

Figures 3(a) and 3(b) show the typical MOKE loops measured along the easy and hard axes for the CoFeB single film at 300 K and the FeRh single film at 400 K, respectively. Figures 3(c) and 3(d) show the corresponding angular dependence of $M_{\mathrm{r}}/M_{\mathrm{s}}$ and H_{c} for the CoFeB and FeRh single films, respectively. The induced fourfold magnetic anisotropy indicates that the cubic magnetocrystalline anisotropy of the epitaxial FeRh layer either in the AFM or FM states can be imprinted into the amorphous CoFeB layer through the AFM/FM and FM/FM interfacial exchange coupling between them. Because the magnetocrystalline anisotropy of FeRh changes from the ⟨110⟩ directions in the AFM state to the ⟨100⟩ directions in the FM state,[39] the easy and hard axes of the induced fourfold anisotropy in the CoFeB layer are swapped with each other after the occurrence of phase transition of FeRh. Comparing the difference in $M_{\mathrm{r}}/M_{\mathrm{s}}$ measured along the easy and hard axes, it is found that the fourfold magnetic anisotropy of the CoFeB layer induced by the AFM FeRh at 300 K is obviously higher than that by the FM FeRh at 400 K. The coercivities for the reference CoFeB/STO(001) film measured along the easy and hard axes are only 8 Oe and 3 Oe, respectively. It is clearly that the exchange coupling to FeRh layer leads to a remarkable enhancement in the coercivity of CoFeB layer. It is well known that the most common phenomena for an AFM/FM bilayer are exchange bias behaviors with the shift in its hysteresis loop and an increasement of its coercivity.[11,12,40] Although we have observed a fourfold magnetic anisotropy and obviously enhanced coercivities in the CoFeB/FeRh bilayer caused by the interfacial exchange coupling regardless of FeRh in the AFM or FM states, there is no shift in hysteresis loops when FeRh is in the AFM state even after a field cooling process. In previously well-studied AFM/FM bilayers, the pinning and rotatable uncompensated moments in the AFM surface may couple to the FM moments across the interface, respectively

leading to the exchange bias field and the increasement of coercivity. The rotatable uncompensated moments can rotate following the FM moments under a magnetic field due to the exchange coupling. The pinned moments have been observed mostly below the rotatable ones. Both kinds of moments are very rare in the commonly used AFM layers, such as IrMn, CoO, *etc*. Synchrotron methods, such as x-ray magnetic circular dichroism, are usually required to detect them.[41,42] Different from these AFM layers, when FeRh is in the AFM state, a great number of residual FM moments can still be observed to be mostly located at the upper and bottom interfaces.[32] They actually can be viewed as the rotatable uncompensated moments distributed in the AFM matrix and well separate the exchange coupling between the below pinned uncompensated moments and the CoFeB moments. Consequently, only the increase of coercivity but no exchange bias is observed in our CoFeB/FeRh bilayer. It should be noted that the residual FM FeRh phase is different from the FM FeRh phase at an elevated temperature. It may display a magnetocrystalline anisotropy collinear with the AFM matrix, but the strength may reduce due to surface defects. Consequently, the fourfold magnetic anisotropy in the CoFeB layer is imprinted from the AFM FeRh surface with a mixture of the residual FM phase and the AFM matrix.

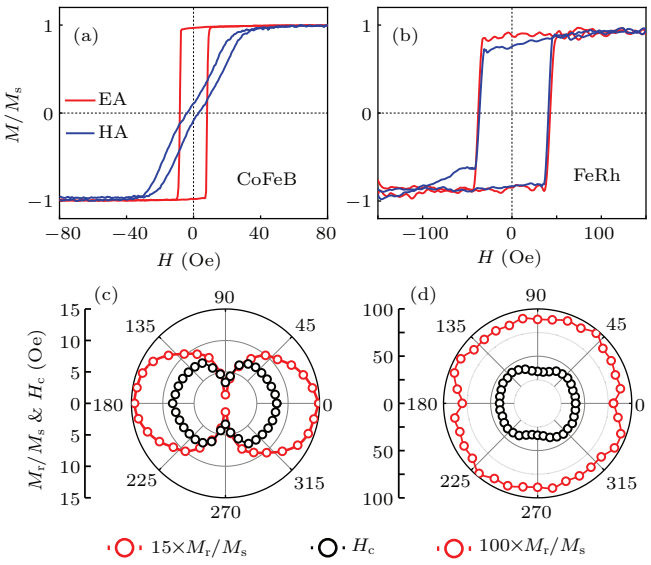

Fig. 3. Hysteresis loops of (a) CoFeB/STO single film at 300 K and (b) FeRh/STO single film at 400 K obtained with an external magnetic field applied along the easy axis (EA) and the hard axis (HA). The corresponding angular dependence of normalized M_r/M_s and H_c of (c) CoFeB/STO film and (d) FeRh/STO film.

The FMR absorption spectra of the bilayer were obtained at different in-plane magnetic field orientations in the temperature range of 300 K–400 K with an interval of 20 K upon heating. Different from the surface characterization method of MOKE, the FMR signal is contributed not only by CoFeB but also by FM FeRh. Figure 4(a) shows a representative spectrum measured at 300 K with an external field H applied along FeRh$[1\bar{1}0]$ ($\varphi = 0°$). The intensity of FMR signal is fitted by the combination of a symmetric Lorentzian term and an antisymmetric dispersive term:[43–45]

$$U = L\frac{\Delta H^2}{(H-H_r)^2+\Delta H^2} + D\frac{\Delta H\,(H-H_r)}{(H-H_r)^2+\Delta H^2} + C, \quad (1)$$

where L and D are the amplitudes of Lorentzian and dispersive parts, respectively. H_r is the resonant field, ΔH is the half-width at half maximum. C is a constant term, which is usually caused by the weak non-resonance mechanism. The experimental data can be well fitted to Eq. (1), the symmetric and antisymmetric contributions are also shown in Fig. 4(a). A pair of H_r and ΔH are extracted. Figure 4(b) displays the H_r measured at different in-plane orientations at various temperatures upon heating, which display a superposition of fourfold and uniaxial contributions over the entire measuring temperature range. At 300 K–340 K, four local minima of H_r are oriented at $\varphi = 0°$, 90°, 180°, 270° and the value of H_r at $\varphi = 0°$ is apparently lower than that at $\varphi = 90°$, confirming the fourfold magnetic anisotropy along FeRh$\langle 110\rangle$ additionally superimposed with a uniaxial magnetic anisotropy along FeRh$[1\bar{1}0]$. At 360 K and higher temperatures, four local minima of H_r are at $\varphi = 45°$, 135°, 225°, 315°, which indicates that the fourfold magnetic anisotropy changes to along FeRh$\langle 100\rangle$. At 360 K and 380 K, the value of H_r at $\varphi = 45°$is lower than that at $\varphi = 135°$, indicates that the uniaxial magnetic anisotropy changes to along FeRh[100]. However, at 400 K it changes back to along FeRh$[1\bar{1}0]$. A simplified Landau-Lifshitz equation is used to quantitatively fit the angular dependence of H_r:[2,39]

$$\left(\frac{2\pi f}{\gamma}\right)^2 = \left[H_r + 4\pi M - \frac{3K_1}{2M} + \frac{2K_u}{M}\cos 2\varphi + \frac{K_1}{2M}\cos 4\varphi\right] \times \left[H_r + \frac{4K_u}{M}\cos 2\varphi + \frac{2K_1}{M}\cos 4\varphi\right], \quad (2)$$

where f is the microwave frequency fixed at 9.3 GHz in the measurements, γ is the gyromagnetic ratio. K_u and K_1 are the in-plane uniaxial and fourfold anisotropy constants, respectively. Figure 4(c) shows the temperature dependence of K_1/M and K_u/M of the bilayer. The K_1/M has a small value of 2.7 Oe at 300 K. It significantly increases when crossing the AFM–FM phase transition temperature and reaches a maximum value of 19.3 Oe at 400 K. The K_u/M has a small value lower than 2 Oe over the entire measuring temperature range. When FeRh is in the AFM state at 300 K, the K_1 and K_u obtained by FMR are the anisotropies of the CoFeB layer. However, when the temperature rises from 300 K to 400 K, the AFM FeRh gradually transfers to FM, which contributes to the FMR signal. Thus, the obtained K_1 and K_u are the anisotropies

of the coupled FM bilayers. The K_1/M of the FeRh single film is also measured as 38.4 Oe at 400 K by FMR, which is significantly larger than the value of the bilayer. Obviously, the exchange coupling to the CoFeB layer can significantly reduce the K_1/M. The orientation of K_u shows a complicated dependence on temperature, which is because of the competition between the different sources. The CoFeB layer itself possesses a uniaxial magnetic anisotropy K_{uCFB}. The ferromagnetic FeRh phase also displays a uniaxial magnetic anisotropy K_{uFeRh}. The exchange coupling between CoFeB and FeRh can additionally induce a uniaxial magnetic anisotropy K_{uex}. When FeRh starts to transfer from AFM to FM, the three components may change with temperatures, resulting in the variation of K_u.

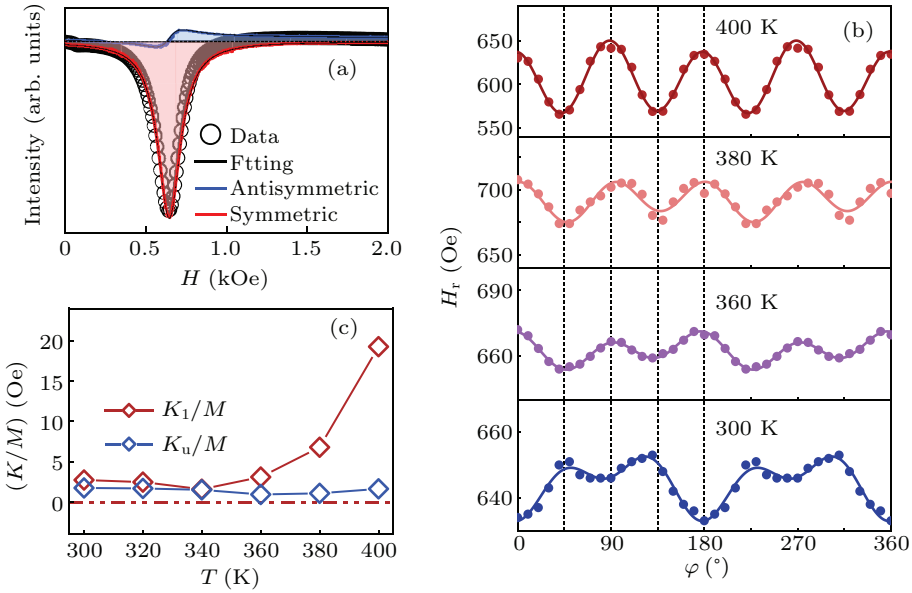

Fig. 4. (a) Representative FMR spectrum (open dots) for the CoFeB/FeRh bilayer measured along FeRh$[1\bar{1}0]$ at 300 K. The corresponding fitting result (black line) consists of the symmetric (red line) and antisymmetric (blue line) parts. (b) The extracted resonance field H_r as a function of the in-plane magnetic field orientation φ at different temperatures. The solid lines are the fitting to Eq. (2). (c) Temperature dependence of the fitting parameters of K_1/M and K_u/M.

Figure 5(a) shows the angular dependence of ΔH for the CoFeB/FeRh bilayer measured in the range of temperature from 300 K to 400 K. Similar to the H_r, they also exhibit a superposition of fourfold and uniaxial symmetries. For the temperature ranged from 300 K to 340 K, the fourfold local minima of ΔH are oriented along FeRh$\langle 110\rangle$, while the uniaxial minima are along FeRh$[1\bar{1}0]$. At 360 K and 400 K, the fourfold local minima of ΔH change to along FeRh$\langle 100\rangle$, while the uniaxial minima keep along FeRh$[1\bar{1}0]$. At these measuring temperatures, the symmetry of ΔH is exactly the same to that of the corresponding H_r. However, at 380 K when the phase transition of FeRh occurs, the fourfold symmetry of ΔH becomes opposite to that of the corresponding H_r. ΔH is often considered to originate from both intrinsic and extrinsic mechanisms. The intrinsic mechanism refers to the contribution of Gilbert damping α, which depends on the microwave frequency f with a relation of $\Delta H^{Gi} = \alpha(2\pi f/\gamma)$.[46–48] Since our FMR measurements are carried out at a fixed frequency, the contribution from Gilbert damping can be considered as a constant, and the periodic change of the angular dependence of ΔH mainly comes from the extrinsic two-magnon scattering (TMS) contribution.[49–51] Thus, the experimentally obtained angular dependence of ΔH can be interpreted by the equation[46,47,52]

$$\Delta H^{\mathrm{Gi+TMS}} \cong \left[\left(\alpha + \frac{\Gamma_0}{2M}\right) + \frac{\Gamma_2}{2M}\cos 2\varphi + \frac{\Gamma_4}{2M}\cos 4\varphi\right]\frac{2\pi f}{\gamma}, \quad (3)$$

where Γ_0, Γ_2, and Γ_4 are the parameters of the constant, twofold, and fourfold terms in the TMS contribution, respectively. The Gilbert damping together with the TMS constant term forms the effective damping and is expressed as $\alpha_{eff} = \alpha + \Gamma_0/2M$, which does not vary with the orientations of applied magnetic field. As shown in Fig. 5(a), the angular dependent linewidth can be well fitted to Eq. (3).

Figure 5(b) shows the fitting parameter of α_{eff} as a function of temperature. When FeRh is in the AFM state, the α_{eff} of the CoFeB/FeRh bilayer is as small as 2.9×10^{-2} at 300 K. When FeRh enters into the FM state, the α_{eff} increases to 5.0×10^{-2} at 400 K. For comparison, the α_{eff} of the CoFeB single film is 1.0×10^{-2} at 300 K, and the α_{eff} of the FeRh single film decreases from 7.9×10^{-2} at 360 K to 5.8×10^{-2} at 400 K. The FMR signal of the nominally AFM FeRh is too weak to be detected when the temperature is below 360 K. It is obviously that the interfacial exchange coupling in the CoFeB/FeRh bilayer can increase the magnetic damping of

the soft CoFeB layer and pull down that of the FM FeRh layer, which is consistent with many previous reports on the enhancement of $\alpha_{\rm eff}$ in FM/AFM systems.[53–56] The $\alpha_{\rm eff}$ displays an anomalously large value of 6.5×10^{-2} at 380 K during the regime of phase transition, which is probably because the AFM FeRh moments stay in an unstable state and can rotates following the FM FeRh moments. This feature is similar to the phenomenon occurred in the FM/AFM exchange biased bilayers, the coercivity displays a peak value when the AFM moments become unstable with reducing the thickness to a critical value.[57]

The fourfold TMS coefficient Γ_4 is as small as 11.9 Oe at 300 K. As FeRh transfers from the AFM to FM states, the Γ_4 remarkably increases to 202.2 Oe at 400 K, as show in Fig. 5(c). The change of the fourfold symmetry of ΔH at 360 K indicates that the direction of the maximum scattering changes from FeRh⟨100⟩ to FeRh⟨110⟩ with the occurrence of the AFM–FM phase transition of FeRh. The twofold TMS coefficient Γ_2 keeps a small value around 6.2 Oe before 340 K and sharply increases to 54.2 Oe at 400 K. Similar to the $\alpha_{\rm eff}$, the Γ_2 also displays an anomalously large value of 105.5 Oe at 380 K when FeRh stays in a mixed AFM–FM state.

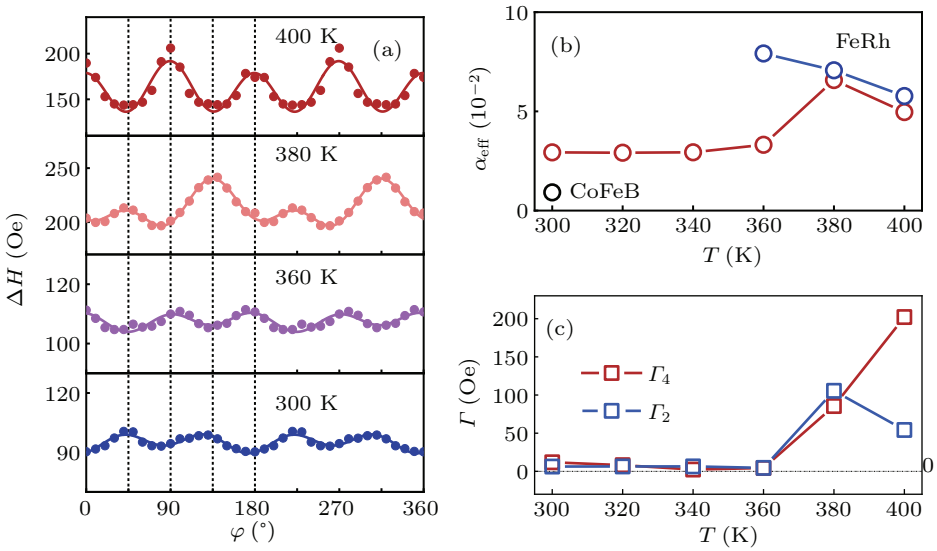

Fig. 5. (a) The linewidth ΔH as a function of the in-plane magnetic field orientation φ at different temperatures for the CoFeB/FeRh bilayer. The solid lines are the fitting to Eq. (3). Temperature dependence of (b) the effective damping coefficients $\alpha_{\rm eff}$ and (c) the TMS coefficients of Γ_4 and Γ_2 for the bilayer. The $\alpha_{\rm eff}$ for the reference CoFeB and FeRh single layers are presented as well.

4. Conclusion

In summary, we fabricated amorphous CoFeB/epitaxial FeRh bilayer on STO(001) substrate. The MOKE measurements indicate that when exchange coupling to the epitaxial FeRh layer, the angular dependence of both $M_{\rm r}/M_{\rm s}$ and $H_{\rm c}$ of CoFeB layer display a fourfold symmetry which both changes with the magnetic phase transition of FeRh layer. The exchange-coupling-induced fourfold magnetic anisotropy of CoFeB layer changes from FeRh⟨110⟩ to FeRh⟨100⟩ directions with a remarkably reduced strength when FeRh transfers from AFM to FM states upon heating. The anisotropic FMR linewidths obtained at different temperatures demonstrate an obviously enhanced effective magnetic damping and the two-magnon scattering as the magnetic phase transition of FeRh occurs. No shift of hysteresis loop or unidirectional magnetic anisotropy was observed the CoFeB/FeRh bilayer even when FeRh is in the AFM state, which is probably because the residual FM FeRh moments located at the interface can well separate the coupling between the pinned FeRh moments and the CoFeB moments.

Acknowledgements

A portion of this work was performed on the Steady High Magnetic Field Facilities, High Magnetic Field Laboratory, Chinese Academy of Sciences.

Project supported by the National Natural Science Foundation of China (Grant Nos. 11874150, 51871233, and 12174103) and the Natural Science Foundation of Shanghai (Grant Nos. 21ZR1420500 and 21JC1402300).

References

[1] Zhan Q F, Vandezande S, Temst K and Van Haesendonck C 2009 *Phys. Rev. B* **80** 094416
[2] Huang Z C, Zhai Y, Lu Y X, Li G D, Wong P K J, Xu Y B, Xu Y X and Zhai H R 2008 *Appl. Phys. Lett.* **92** 113105
[3] Ahmad E, Lopez-Diaz L, Gu E and Bland J A C 2000 *J. Appl. Phys.* **88** 354
[4] Dai G H, Zhan Q F, Liu Y W, Yang H L, Zhang X S, Chen B and Li R W 2012 *Appl. Phys. Lett.* **100** 122407
[5] Tang Z H, Wang B M, Yang H L, Xu X Y, Liu Y W, Sun D D, Xia L X, Zhan Q F, Chen B, Tang M H, Zhou Y C, Wang J L and Li R W 2014 *Appl. Phys. Lett.* **105** 103504
[6] Berkowitz A E and Takano K 1999 *J. Magn. Magn. Mater.* **200** 552
[7] Carey M J, Berkowitz A E, Borchers J A and Erwin R W 1993 *Phys. Rev. B* **47** 9952
[8] Nogues J and Schuller I K 1999 *J. Magn. Magn. Mater.* **192** 203

[9] Parkin S S P, Roche K P, Samant M G, Rice P M, Beyers R B, Scheuerlein R E, O'Sullivan E J, Brown S L, Bucchigano J, Abraham D W, Lu Y, Rooks M, Trouilloud P L, Wanner R A and Gallagher W J 1999 *J. Appl. Phys.* **85** 5828

[10] Chu Y H, Martin L W, Holcomb M B, Gajek M, Han S J, He Q, Balke N, Yang C H, Lee D, Hu W, Zhan Q, Yang P L, Fraile-Rodriguez A, Scholl A, Wang S X and Ramesh R 2008 *Nat. Mater.* **7** 678

[11] Zhan Q F and Krishnan K M 2010 *Appl. Phys. Lett.* **96** 112506

[12] Zhang W, Bowden M E and Krishnan K M 2011 *Appl. Phys. Lett.* **98** 092503

[13] Fullerton E E, Jiang J S and Bader S D 1999 *J. Magn. Magn. Mater.* **200** 392

[14] Zeng H, Li J, Liu J P, Wang Z L and Sun S H 2002 *Nature* **420** 395

[15] Liu J P, Luo C P, Liu Y and Sellmyer D J 1998 *Appl. Phys. Lett.* **72** 483

[16] Kouvel J S and Hartelius C C 1962 *J. Appl. Phys.* **33** 1343

[17] Moruzzi V L and Marcus P M 1992 *Phys. Rev. B* **46** 2864

[18] Annaorazov M P, Nikitin S A, Tyurin A L, Asatryan K A and Dovletov A K 1996 *J. Appl. Phys.* **79** 1689

[19] Sharma M, Aarbogh H M, Thiele J U, Maat S, Fullerton E E and Leighton C 2011 *J. Appl. Phys.* **109** 083913

[20] Thiele J U, Maat S and Fullerton E E 2003 *Appl. Phys. Lett.* **82** 2859

[21] Jen S U, Yao Y D, Chen Y T, Wu J M, Lee C C, Tsai T L and Chang Y C 2006 *J. Appl. Phys.* **99** 053701

[22] Fuji Y, Kaji S, Hara M, Higashi Y, Hori A, Okamoto K, Nagata T, Baba S, Yuzawa A, Otsu K, Masunishi K, Ono T and Fukuzawa H 2018 *Appl. Phys. Lett.* **112** 062405

[23] Ikeda S, Miura K, Yamamoto H, Mizunuma K, Gan H D, Endo M, Kanai S, Hayakawa J, Matsukura F and Ohno H 2010 *Nat. Mater.* **9** 721

[24] Paluskar P V, Kohlhepp J T, Swagten H J M, Koopmans B, Wolters R, Boeve H and Snoeck E 2007 *J. Phys. D: Appl. Phys.* **40** 1234

[25] Wang D, Nordman C, Daughton J M, Qian Z, Fink J, Wang D, Nordman C, Daughton J M, Qian Z and Fink J 2004 *IEEE T. Magn.* **40** 2269

[26] M, Komiyama K, Shirota Y, Fujiwara Y, Tsunashima S and Matsuuras 1997 *J. Magn. Magn. Mater.* **165** 308

[27] Feng T and Childress J R 1999 *J. Appl. Phys.* **85** 4937

[28] Oguz K and Coey J M D 2009 *J. Magn. Magn. Mater.* **321** 1009

[29] Mizuguchi M, Suzuki Y, Nagahama T and Yuasa S 2007 *Appl. Phys. Lett.* **91** 012507

[30] Kipgen L, Fulara H, Raju M and Chaudhary S 2012 *J. Magn. Magn. Mater.* **324** 3118

[31] Maat S, Thiele J U and Fullerton E E 2005 *Phys. Rev. B* **72** 214432

[32] Fan R, Kinane C J, Charlton T R, Dorner R, Ali M, de Vries M A, Brydson R M D, Marrows C H, Hickey B J, Arena D A, Tanner B K, Nisbet G and Langridge S 2010 *Phys. Rev. B* **82** 184418

[33] Pressacco F, Uhliotar V, Gatti M, Bendounan A, Fullerton E E and Sirotti F 2016 *Sci. Rep.* **6** 22383

[34] Ding Y, Arena D A, Dvorak J, Ali M, Kinane C J, Marrows C H, Hickey B J and Lewis L H 2008 *J. Appl. Phys.* **103** 07B515

[35] Suzuki I, Koike T, Itoh M, Taniyama T and Sato T 2009 *J. Appl. Phys.* **105** 07E501

[36] Han G C, Qiu J J, Yap Q J, Luo P, Laughlin D E, Zhu J G, Kanbe T and Shige T 2013 *J. Appl. Phys.* **113** 17C107

[37] Xie Y L, Zhan Q F, Shang T A, Yang H L, Wang B M, Tang J and Li R W 2017 *AIP Adv.* **7** 056314

[38] Kim C G, Rheem Y W, Kim C O, Shalyguina E E and Ganshina E A 2003 *J. Magn. Magn. Mater.* **262** 412

[39] Xie Y, Zhan Q, Hu Y, Hu X, Chi X, Zhang C, Yang H, Xie W, Zhu X, Gao J, Cheng W, Jiang D and Li R W 2020 *NPG Asia Mater.* **12** 67

[40] Stiles M D and McMichael R D 2001 *Phys. Rev. B* **63** 064405

[41] Chang Y C, Hsiao S N, Liu S H, Su S H, Chiu K F, Hsieh W C, Chen S K, Lin Y G, Lee H Y, Sung C K and Duh J G 2015 *J. Appl. Phys.* **117** 17D154

[42] Tomiyasu K, Inami T and Ikeda N 2004 *Phys. Rev. B* **70** 184411

[43] Bai L H, Gui Y S, Wirthmann A, Recksiedler E, Mecking N, Hu C M, Chen Z H and Shen S C 2008 *Appl. Phys. Lett.* **92** 032504

[44] Qiao S, Nie S, Zhao J, Huo Y, Wu Y and Zhang X 2013 *Appl. Phys. Lett.* **103** 152402

[45] Mecking N, Gui Y S and Hu C M 2007 *Phys. Rev. B* **76** 224430

[46] Ruiz-Calaforra A, Bracher T, Lauer V, Pirro P, Heinz B, Geilen M, Chumak A V, Conca A, Leven B and Hillebrands B 2015 *J. Appl. Phys.* **117** 163901

[47] Chen Z, Kong W, Mi K, Chen G, Zhang P, Fan X, Gao C and Xue D 2018 *Appl. Phys. Lett.* **112** 122406

[48] Zhao Y, Song Q, Yang S H, Su T, Yuan W, Parkin S S P, Shi J and Han W 2016 *Sci. Rep.* **6** 22890

[49] Mizukami S, Watanabe D, Oogane M, Ando Y, Miura Y, Shirai M and Miyazaki T 2009 *J. Appl. Phys.* **105** 07D306

[50] Infante I C, Osso J O, Sanchez F and Fontcuberta J 2008 *Appl. Phys. Lett.* **92** 012508

[51] Dubowik J, Zaleski K, Glowinski H and Goscianska I 2011 *Phys. Rev. B* **84** 184438

[52] Belmeguenai M, Tuzcuoglu H, Gabor M S, Petrisor T, Tiusan C, Berling D, Zighem F, Chauveau T, Chérif S M and Moch P 2013 *Phys. Rev. B* **87** 184431

[53] McCord J, Mattheis R and Elefant D 2004 *Phys. Rev. B* **70** 094420

[54] Le Graet C, Spenato D, Pogossian S P, Dekadjevi D T and Ben Youssef J 2010 *Phys. Rev. B* **82** 100415

[55] Weber M C, Nembach H, Hillebrands B and Fassbender J 2005 *J. Appl. Phys.* **97** 10A701

[56] McCord J, Kaltofen R, Schmidt O G and Schultz L 2008 *Appl. Phys. Lett.* **92** 162506

[57] Tang Y J, Roos B F P, Mewes T, Frank A R, Rickart M, Bauer M, Demokritov S O, Hillebrands B, Zhou X, Liang B Q, Chen X and Zhan W S 2000 *Phys. Rev. B* **62** 8654